Faraday Discussions
Cite this: *Faraday Discuss.*, 2025, **258**, 265

PAPER

Arctic tropospheric ozone seasonality, depletion, and oil field influence†

Evelyn M. Widmaier, ‡§[a] Andrew R. Jensen §[a] and Kerri A. Pratt *[ab]

Received 7th October 2024, Accepted 19th November 2024
DOI: 10.1039/d4fd00166d

Near-surface tropospheric ozone depletion events (ODEs) occur in the polar regions during springtime when ozone reacts with bromine radicals, driving tropospheric ozone mole ratios below 15 ppb (part-per-billion; nmol mol^{-1}). ODEs alter atmospheric oxidative capacity by influencing halogen radical recycling mechanisms and the photochemical production of hydroxyl radicals (•OH). Herein, we examined five years of continuous ozone measurements at two coastal Arctic sites: Utqiaġvik, Alaska and ~260 km southeast at Oliktok Point, within the North Slope of Alaska oil fields. These data informed seasonal ozone trends, springtime ozone depletion, and the influence of oil field combustion emissions. Ozone depletion occurred frequently during spring: 35% of the time at Utqiaġvik and 40% at Oliktok Point. ODEs often occurred concurrently at both sites (40–92% of observed ODEs per year), supporting spatially widespread ozone depletion. Observed ozone depletion timescales are consistent with transport of ozone-depleted air masses, suggesting regional active bromine chemistry. Local-scale ozone depletion affecting individual sites occurred less frequently. Ozone depletion typically coincided with calm winds and had no clear dependence on temperature. Consistently lower ozone mole ratios year-round at Oliktok Point, compared to Utqiaġvik, indicate local-scale ozone titration within the stable boundary layer by nitric oxide (NO•) combustion emissions in the Arctic oil fields. Oxidation of combustion-derived volatile organic compounds in the presence of NO_x also likely contributes to ozone formation downwind, for example at Utqiaġvik, pointing to complex local and regional impacts of combustion emissions as Arctic anthropogenic activity increases.

[a]*Department of Chemistry, University of Michigan, Ann Arbor, MI, USA. E-mail: prattka@umich.edu*
[b]*Department of Earth and Environmental Sciences, University of Michigan, Ann Arbor, MI, USA*

† Electronic supplementary information (ESI) available: Ozone observations, illustration of ODE definitions, wind rose plots, HYSPLIT backward air mass trajectories, temperature observations, ODE timescales and durations. See DOI: **https://doi.org/10.1039/d4fd00166d**

‡ Now at: Department of Chemistry, University of Wisconsin, Madison, WI, USA.

§ Contributed equally.

1 Introduction

Ozone is the third most potent anthropogenic greenhouse gas after carbon dioxide and methane.[1] It also plays a central role in atmospheric oxidation as the primary precursor to the hydroxyl radical ($^{\bullet}OH$),[2,3] the main oxidant responsible for the removal of many trace gases emitted into the atmosphere.[4,5] Average annual Arctic ozone mole ratios range from 20–50 ppb (parts-per-billion, nmol mol^{-1}; typically ~30 ppb) at monitoring stations across the Arctic.[6,7] Arctic surface-level ozone mole ratios are reduced below 15 ppb during frequent ozone depletion events (ODEs) in the polar spring following the first sunrise after polar night (>24 hours of darkness). These ODEs are due to multiphase photocatalytic bromine chemistry (R1–R4).[8–11]

$$Br_{2(g)} + h\nu \rightarrow 2Br^{\bullet}_{(g)} \quad (R1)$$

$$Br^{\bullet}_{(g)} + O_{3(g)} \rightarrow BrO^{\bullet}_{(g)} + O_{2(g)} \quad (R2)$$

$$BrO^{\bullet}_{(g)} + HO_2{}^{\bullet}_{(g)} \rightarrow HOBr_{(g)} + O_{2(g)} \quad (R3)$$

$$HOBr_{(aq)} + Br^{-}_{(aq)} + H^{+}_{(aq)} \rightarrow Br_{2(g)} + H_2O_{(l)} \quad (R4)$$

Molecular bromine (Br_2) originates from photochemical snowpack[12–14] and aerosol production.[15,16] Br_2 has a photolysis lifetime of tens of seconds in the springtime Arctic[17] and photolyzes to produce bromine radicals ($Br^{\bullet}$; R1).[11] Bromine radicals react with ozone to form bromine monoxide ($BrO^{\bullet}$), depleting ozone in the process (R2).[8,11,18] $BrO^{\bullet}$ reacts with the hydroperoxyl radical ($HO_2{}^{\bullet}$) to produce hypobromous acid (HOBr; R3).[11,19] HOBr can then undergo heterogeneous uptake to the snowpack or aerosol surface to oxidize bromide (Br^{-}), producing Br_2 (R4), which reinitiates the "bromine explosion" cycle in which atmospheric bromine rapidly increases to deplete ozone.[5,11,20] Following an ODE, surface-level ozone may be replenished *via* vertical mixing[21–25] and/or advection of non-depleted air masses.[26]

Kinetic studies based on observations of $BrO^{\bullet}$ estimate that bromine-driven ozone depletion chemistry occurs on the order of days.[27–30] Observations of shorter (≤24 h) ozone depletion timescales (the time for ozone to fall from atmospheric background mole ratios to below 15 ppb and reach a minimum) suggest air mass transport mechanisms in which ozone-depleted air is transported to the measurement site from elsewhere.[5,31–33] Often, these air masses have trajectories over snow-covered first-year sea ice,[34–37] which is typically associated with elevated $BrO^{\bullet}$ mole ratios.[38–41] Peterson *et al.*[42] also reported elevated $BrO^{\bullet}$ up to 200 km inland during flights near Utqiaġvik, Alaska, with the highest $BrO^{\bullet}$ observations occurring over snow-covered tundra rather than sea ice.

Several studies have investigated springtime ODE spatial scales using monitoring networks, modelling, and research flights. Using ground-based measurements at coastal sites and several research cruises, Jacobi *et al.*[26] argued that depletion of near-surface ozone (<5 ppb) is typical and widespread. Similarly, chemical transport models suggest that large areas of the Arctic, >50% of northern high latitudes (>70° N), are ozone-depleted (<20 ppb) during springtime.[40,41] Peterson *et al.*[24] examined ozone levels at coastal Utqiaġvik, AK, and

inland Atqasuk, finding that two-thirds of all ODEs (O_3 < 10 ppb) occurred concurrently and that those ODEs extended at least the ~90 km distance between the sites. Similarly, Van Dam *et al.*[43] observed concurrent ODEs (O_3 < 15 ppb) at Utqiaġvik and Toolik Lake, ~400 km to the southeast and ~200 km inland. Arctic flights in April found ozone-depleted air masses spanning 130 km at 50 m altitude[44] and 1000 km at 305 m altitude.[45] Ridley *et al.*[46] observed ODEs (O_3 < 20 ppb) during March–May spanning ~300 km over flight paths at 30 m altitude and up to ~900 km using a combination of *in situ* flight observations at 30 m altitude and lidar remote sensing at 4–8 km altitude. Halfacre *et al.*[31] estimated the spatial scale of a single ODE (O_3 < 15 ppb) as ~877 km (median diameter; range of ~200–3500 km) based on the distance travelled by modelled air mass trajectories during ODEs observed by buoys in the Arctic Ocean. For more complete ODEs (O_3 < 10 ppb), Halfacre *et al.*[31] estimated spatial scales of ~282 km. Using satellite remote sensing, Platt and Wagner[47] and Seo *et al.*[48] observed elevated Arctic BrO$^\bullet$ vertical column densities with spatial scales of 300–2000 km (lasting 1–3 days) and ~500–1500 km, respectively, suggesting similarly widespread Arctic reactive bromine chemistry.

Nitrogen oxides (NO_x = NO$^\bullet$ + $NO_2^\bullet$) also perturb ozone and halogen chemistry. NO$^\bullet$ reacts with (titrates) ozone at night to form $NO_2^\bullet$ and molecular oxygen (R5), while $NO_2^\bullet$ photolysis contributes to daytime ozone production.[49] Previous measurements at Ny-Ålesund, Svalbard observed reduced ozone mole ratios downwind of a diesel power plant emitting NO$^\bullet$.[50] Photochemical snowpack NO_x emissions have been shown to be coupled to reactive halogens.[51,52] In NO_x-polluted environments, BrO$^\bullet$ can react with $NO_2^\bullet$ to form bromine nitrate ($BrONO_2$; R6) as a reservoir for reactive bromine and an alternative pathway for reactive bromine recycling.[53,54] Wang and Pratt[55] found R6 to be competitive with R3 (reaction with HO_2) even under low $NO_2^\bullet$ (<0.05 ppb) conditions. Hydrolysis of $BrONO_2$ on acidic surfaces forms HOBr (R7),[56–58] which is then available to regenerate Br_2 (R4). In a numerical modeling study, Cao *et al.*[53] found that $BrONO_2$ production (at 0.015 ppb NO_x) accelerated ozone depletion by forming HOBr (R7). Anthropogenic NO_x emissions have been observed in the Russian Arctic, including from urban,[59] shipping,[60] and oil and gas production sources.[61] Above the oil fields on the North Slope of Alaska, elevated NO_2 mole ratios were observed coincidentally with reduced BrO$^\bullet$.[62,63] A modeling study by Custard *et al.*,[62] constrained by observations at Utqiaġvik, AK, showed that elevated NO_x mole ratios (0.7–1.6 ppb) suppressed HOBr formation and slowed ozone depletion relative to background NO_x mole ratios (0.05–0.1 ppb). These interactions between NO_x and reactive bromine recycling *versus* suppression still require further investigation. Regardless of its impact on reactive bromine chemistry, elevated NO_x is expected to titrate ozone (R5) in this stable boundary layer with elevated combustion emissions, as observed during flights over the Alberta oil sands.[64]

$$NO^\bullet_{(g)} + O_{3(g)} \rightarrow NO_2^\bullet{}_{(g)} + O_{2(g)} \quad \text{(R5)}$$

$$BrO^\bullet_{(g)} + NO_2^\bullet{}_{(g)} \rightarrow BrONO_{2(g)} \quad \text{(R6)}$$

$$BrONO_{2(aq)} + H_2O_{(l)} \rightarrow HOBr_{(aq)} + HNO_{3(aq)} \quad \text{(R7)}$$

The North Slope of Alaska (NSA) is home to the Prudhoe Bay and Kuparuk River oil fields which produced 7.9 and 2.9 million barrels of oil in 2013, respectively, making them the third and sixth largest oil fields in North America as of that year.[65] NSA industrial fuel combustion, used in part to power the oil drilling platforms, is estimated to account for ~31 000 tons of annual NO_x emissions according to the 2017 National Emissions Inventory.[66] Satellite remote sensing studies have reported strong, local NO_x emissions from oil and gas production in the Arctic.[67–69] Studies at Oliktok Point, located within the Kuparuk River oil field, have observed constant influence from oil field emissions, including NO_x and particulate matter, due to local combustion emissions from oil and gas extraction activities.[70–72] Utqiaġvik also experiences NO_x pollution, although intermittently, due to air mass transport from the town of Utqiaġvik, ~5 km to the southwest, as well as the NSA oil fields, ~300 km to the southeast.[62,73–75]

There are uncertainties regarding the interactions between ozone, reactive bromine, and anthropogenic pollution as they relate to ozone depletion and atmospheric oxidative capacity in the Arctic. The role of NO_x in modulating Arctic ozone is poorly constrained and is expected to grow in importance as development and anthropogenic emissions in the Arctic increase.[76–78] In this study, we analyze five years (2016–2021) of continuous ozone and meteorology data at Utqiaġvik (formerly known as Barrow) and Oliktok Point, Alaska, to examine seasonal ozone trends, as well as ODE spatial scales, timescales, and depletion mechanisms. Oliktok Point is within the NSA oil fields and is located ~260 km from Utqiaġvik, which mainly experiences clean air masses from the Beaufort Sea. These two sites are within the estimated spatial scale of a singular ODE,[31] but differ in the local abundance of NO_x emissions, providing insight into the influence of anthropogenic NO_x on tropospheric ozone chemistry in the present and future Arctic.

2 Methods

2.1 Ozone and meteorological data

Ozone mole ratios, temperature, wind speed, and wind direction were measured by the National Oceanic and Atmospheric Administration Global Monitoring Laboratory Barrow Atmospheric Baseline Observatory (NOAA GML BRW) at Utqiaġvik, Alaska (71.323° N, 156.611° W; 8 m above sea level)[79] and the Department of Energy Atmospheric Radiation Measurement (DOE ARM) facility at Oliktok Point, Alaska (70.495° N, 149.886° W; 10 m above sea level).[80,81] Both the Utqiaġvik and Oliktok Point sites are coastal, situated ~2 km and <1 km from the ocean, respectively.

Hourly ozone data and collocated meteorological data were available at both sites between 7 August 2016 and 20 April 2021. At both sites, ozone was measured using ultraviolet ozone analyzers (Thermo Scientific; model 49C until 31 December 2020, then model 49i thereafter at Utqiaġvik; model 49i at Oliktok Point), with a reported limit of detection (LOD) of 0.5 ppb at 60 s averaging. Ambient air was sampled at 6 m above ground level (AGL) at Utqiaġvik and 10 m AGL at Oliktok Point. Ozone measurements below 0.5 ppb were replaced with 0.5 ppb for calculations. Note that this choice of 0.5 ppb may bias ozone levels slightly high during complete ODEs, but this is not expected to change the findings herein. Daily average ozone mole ratios for the full study period are presented in Fig. S1.†

At Utqiaġvik, temperature was measured using a platinum resistance thermometer (Logan, model 4159) at 10 m AGL. Wind speed and wind direction at Utqiaġvik were measured at 10 m AGL using a 2D mechanical anemometer (RM Young, model 05103-12) between 7 August 2016 and 24 September 2017, and a 2D sonic anemometer (Lufft, model Ventus-UMB) between 25 September 2017 and 20 April 2021. All meteorological parameters at Oliktok Point were measured at 10 m AGL using a weather transmitter (Vaisala, model WXT520).

For the analysis herein, seasons were considered as follows: winter (1 November–31 January), spring (1 February–15 May), summer (16 May–31 July), and fall (1 August–31 October). Broadly, these categorizations are based on the observed ozone temporal trends as discussed in Section 3.1. Spring is primarily defined based on polar sunrise, which initiates active bromine chemistry and ozone depletion,[8] and with the end based on the typical start of snowmelt, which is associated with the shutdown of active bromine chemistry.[82,83] The transition between the end of summer and beginning of fall corresponds to solar radiation falling in early August to ~50% of the annual maximum.[84,85] The start of winter is chosen as shortly before the start of polar night, which corresponds to days with >24 hours of darkness and occurred each year approximately from 19 November–22 January at Utqiaġvik and 22 November–18 January at Oliktok Point.

2.2 Identification of ozone depletion events

Springtime ozone depletion event (ODE) characteristics were calculated following the definitions used by Halfacre *et al.*,[31] as illustrated in Fig. S2.† ODEs are defined as time periods when the ozone mole ratio ($[O_3]$) dropped below 15 ppb for at least 2 h. ODE timescales are defined relative to the local maximum $[O_3]$ preceding the ODE ($[O_3]_{max}$) and the observed minimum mole ratio during the ODE ($[O_3]_{min}$). The ODE start time (ODE_{start}) is when $[O_3]$ first falls below 90% of the value of the mole ratio range ($[O_3]_{min}$ to $[O_3]_{max}$) during an ODE. The ODE has ended after $[O_3]$ recovers above 20 ppb for at least 12 hours. The ODE stop time (ODE_{stop}) is when $[O_3]$ recovers to 90% of the local maximum following the ODE and does not need to be 12 hours after rising above the recovery threshold of 20 ppb. This threshold differs from the 25 ppb threshold used by Halfacre *et al.*[31] due to lower observed average springtime ozone mole ratios, particularly at Oliktok Point as discussed in Section 3.3 (24.7 ± 0.2 ppb at Utqiaġvik and 21.8 ± 0.2 ppb at Oliktok Point; ±95% confidence intervals). For the calculation of ozone depletion timescales (τ_{O_3}), the ozone decrease stop time (ODE_{dec}) is defined as when $[O_3]$ first falls below 10% of the value of the mole ratio range during an ODE. The ozone depletion timescale is represented by negative inverse slope of the natural logarithm of $[O_3]$ *versus* time during the period between ODE_{start} and ODE_{dec}. The total ODE duration is defined as the difference between ODE_{stop} and ODE_{start}. For ODEs spanning the transition between seasons (4 ODEs at Utqiaġvik and 7 ODEs at Oliktok Point), the ODEs are assigned based on ODE_{start}.

Periods of depleted ozone were also observed throughout the year. Since "ODEs" are associated with springtime, bromine-driven ozone depletion,[8] we do not use this term when referring to ozone depletion outside of spring. However, the same definitions as used with ODEs were used to identify and characterize ozone depletion outside of spring.

2.3 Backward air mass trajectory modeling

The backward air mass trajectories for two ODEs (beginning February 20 and March 1, 2020) were investigated using version 4 of the Hybrid Single-Particle Lagrangian Integrated Trajectory (HYSPLIT) model[86–88] and 1° meteorology data from the National Oceanic and Atmospheric Administration (NOAA)/National Centers for Environmental Prediction (NCEP) Global Data Assimilation System (GDAS).[89] GDAS is divided into 23 vertical layers (pressure levels), with ground-level layers (<900 mbar) having a 25 mbar resolution. Results were visualized in the Quantum Geographic Information System (QGIS) software (version 3.34.10).[90]

We implement the HYSPLIT model in a similar manner as Halfacre *et al.*[31] The air mass trajectories were initialized at the measurement sites at a height of 6 m AGL for Utqiaġvik and 10 m for Oliktok Point, corresponding to the heights of the ozone measurements. Additional trajectories were modelled at 50 m AGL for both sites, yielding negligible differences. The vertical resolution of the GDAS meteorological data (25 mbar) suggests the HYSPLIT backward air mass trajectories are insensitive to near-surface starting heights. Each ODE_{stop} time was used as the beginning of the air mass trajectory, and the run lengths were based on the ODE durations. We present isobaric trajectories as ODEs typically occur in a stable surface layer isolated from air aloft.[10,91] Due to large uncertainties in these air mass trajectories from a general lack of meteorological measurements in the region,[92,93] we interpreted them broadly (*i.e.*, general direction of the air mass origin).

3 Results and discussion

3.1 Seasonal ozone trends

Seasonal (Fig. 1a and S3a†) and monthly (Fig. 1b) ozone mole ratios at Utqiaġvik for August 2016 to April 2021 agree with previously reported observations of high winter ozone, variable springtime ozone due to ODEs, low summer ozone, and increasing ozone in the fall.[6,7,10,94] Mean ozone mole ratios were statistically

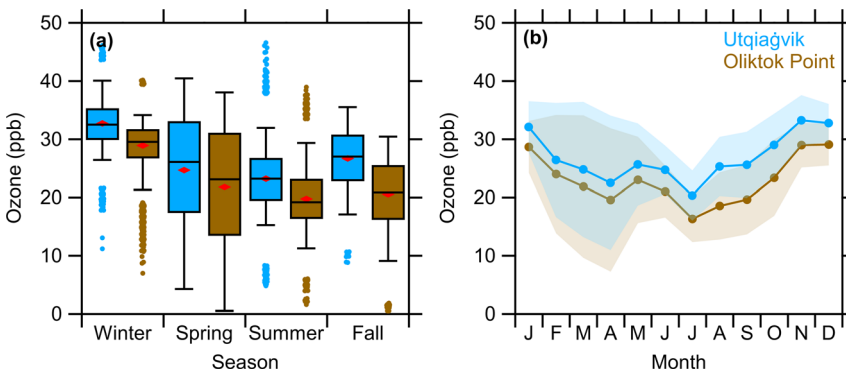

Fig. 1 (a) Seasonal ozone distributions and (b) monthly average ozone mole ratios (ppb) at Utqiaġvik and Oliktok Point from 2016–2021 using hourly averaged mole ratios. The boxes and whiskers in (a) show 5th, 25th, 50th (median), 75th, and 95th percentiles. The red diamond markers represent the seasonal averages. Outliers are shown as separate markers. Shading in (b) represents 1 standard deviation for data across all years.

different (95% confidence) between the seasons. Seasonal average ozone mole ratios at Utqiaġvik (±95% confidence intervals) were at a maximum during winter (average of 32.71 ± 0.08 ppb) due to the lack of bromine photochemistry during the polar night.[18] The spring polar sunrise initiates reactive bromine photochemistry, resulting in ODEs and lower average ozone mole ratios compared to winter (average of 24.7 ± 0.2 ppb).[8,15,95,96] The spring minimum occurred in April (average of 22.5 ± 0.4 ppb; Fig. 1b), as previously observed at Utqiaġvik.[7,10] Summer average ozone mole ratios represent the annual minimum (average of 23.2 ± 0.1 ppb), specifically in July (average of 20.3 ± 0.2 ppb). Summertime ozone minima are common in remote environments due to net photochemical destruction.[97–101] Fall ozone mole ratios at Utqiaġvik (average of 26.7 ± 0.1 ppb) were higher than in spring and summer. Monthly averages over the duration of the study period at Utqiaġvik were not statistically different (95% confidence) from those reported for 1973–1984 by Oltmans and Komhyr[7] and for 1999–2008 by Oltmans *et al.*,[10] except for August, which was 5 ± 5 ppb lower during the former study compared to this study. This overall agreement suggests this study period (2017–2021) is representative of historical seasonal ozone behavior at Utqiaġvik.

The Oliktok Point site is ~260 km to the southeast of Utqiaġvik and also on the northern coast of Alaska. Predominant wind directions were from the east and northeast (Beaufort Sea) at both sites, with additional contributions from the southwest over snow-covered tundra at Oliktok Point in winter and spring (Fig. S5†). Temperatures were strongly correlated ($R^2 = 0.93$; Fig. S6†) between the sites. However, temperatures at Oliktok Point were statistically lower than those at Utqiaġvik in the winter and spring by 0.6 °C and 0.06 °C, respectively, and higher in the summer and fall by 1 °C and 0.3 °C, respectively. Average wind speeds (±95% confidence intervals) at Oliktok Point (6.67 ± 0.03 m s^{-1}) were statistically higher throughout the year compared to Utqiaġvik (5.86 ± 0.03 m s^{-1}) by 0.81 ± 0.05 m s^{-1} (range of 0.61 ± 0.08 to 1.01 ± 0.08 m s^{-1} for individual seasons). While these meteorological conditions have minor differences, they are not expected to make significant differences in overall ozone mole ratios and temporal trends compared to other local factors, as discussed below.

Ozone mole ratios at Oliktok Point from August 2016 to April 2021 followed similar seasonal and monthly trends as those observed at Utqiaġvik (Fig. 1). Daily averaged ozone mole ratios correlated between the two sites ($R^2 = 0.62$; Fig. S4†), suggesting similar regional ozone behavior. However, ozone was statistically lower (95% confidence) during every season and every month at Oliktok Point compared to Utqiaġvik. Average (±95% confidence intervals) ozone mole ratios at Oliktok Point were 28.90 ± 0.08 ppb in winter, 21.8 ± 0.2 ppb in spring, 19.7 ± 0.1 ppb in summer, and 20.5 ± 0.1 ppb in fall. The springtime and summer minima occurred in April (19.5 ± 0.4 ppb) and July (16.3 ± 0.1 ppb), respectively, as was observed at Utqiaġvik. Overall, the similar temporal trends between Utqiaġvik and Oliktok Point suggest similar regional ozone behavior, with the consistently lower mole ratios at Oliktok Point likely due local anthropogenic NO_x influence, as discussed in Section 3.3.

While bromine chemistry drives springtime ozone loss,[11] iodine chemistry has been identified as another significant ozone sink in the Arctic.[102,103] Iodine chemistry is active throughout the sunlit period (spring–fall), with iodine monoxide ($IO^{\bullet}$) mole ratios and calculated ozone loss in the central Arctic Ocean peaking in March–April and July–August.[102] Sturges and Barrie[104] observed similar

spring and fall maxima in particulate iodine at sites in the Canadian Arctic (Alert and Mould Bay). Notably, fall ozone mole ratios at Oliktok Point were lower than in the spring, in contrast to observations at Utqiaġvik where ozone mole ratios were higher in fall than in spring. Thus, these seasonal iodine trends may contribute to the lower fall ozone mole ratios at Oliktok Point through reactive iodine recycling, depending on the contributions from interactions with NO_x pollution (discussed in Section 3.3). Additionally, the oil fields may also serve as an additional source of iodine. Iodine-rich brines have been identified in oilwell produced water, and iodine content aids petroleum resource identification.[105–108] However, we are not aware of any reports of iodine in produced water or the atmosphere in the NSA oil fields, and therefore, this potential is speculative. Therefore, further studies are needed to understand the interactions between iodine, NO_x, and ozone depletion.

NO_x and volatile organic compound (VOC) emissions from oil and gas extraction activities can yield ozone production downwind.[109,110] In the presence of NO_x, VOC photooxidation produces ozone.[111–113] Fresh NO˙ emissions near Oliktok Point titrate local ozone (R5), as discussed further in Section 3.3, but these emissions may yield net ozone formation as the air mass is transported downwind to Utqiaġvik. At the Zotino Tall Tower Observatory in central Siberia, Moiseenko *et al.*[114] observed net ozone production, which they attributed to an abundance of biogenic VOCs, as well as a mixture of soil, biomass burning, and anthropogenic NO_x emissions. During the fall, wind directions at Utqiaġvik came from the southeast, in the direction of the NSA oil fields, for ~15% of the time (Fig. S5†). Ozone production in these air masses may potentially explain the higher ozone mole ratios at Utqiaġvik in the fall compared to spring, whereas ozone mole ratios were higher in spring than in fall at Oliktok Point. At Alert, Canada, Gautrois *et al.*[115] observed annual minimum hydrocarbon mole ratios (*e.g.*, methane, *n*-hexane, benzene) in July and August. At Villum Research Station, Greenland, Pernov *et al.*[116] found significant VOC contributions from biomass burning in the fall, the marine cryosphere (*e.g.*, emissions during snowmelt) in the summer, and Arctic haze in the spring. Although studies have shown seasonal cycles of VOCs in the remote Arctic,[115,116] detailed measurements of VOC emissions from oil and gas activities are necessary to assess their relative contribution to local and regional VOC mole ratios, as well as their potential to form ozone.

3.2 Springtime ozone depletion events

Ozone was frequently depleted at Utqiaġvik and Oliktok Point during springtime (Fig. 1a). From 2017–2021, a total of 58 springtime ODEs (range of 9–14 per year, annual median of 11) were identified at Utqiaġvik, while 60 ODEs (8–16 per year, annual median of 10) were identified at Oliktok Point. It is worth noting that the spring 2021 data used in this study ends on 20 April, likely missing some springtime ODEs for that year. For context, 1–5 ODEs occurred between 20 April and 15 May during previous years. Ozone at Utqiaġvik was depleted (as defined in Section 2.2) for 35% of the springtime data considered in this study, ranging from 18–56% of the data during individual years. Oliktok Point experienced more ozone depletion overall, with ODEs covering 40% of all springtime data (24–61% for individual years). The prevalence of ODEs along the north coast of Alaska indicates frequent, regional ozone depletion. In comparison, Halfacre *et al.*[31]

reported observations of ozone-depleted air for ~60–65% of springtime at buoys in the Arctic Ocean.

Observations of springtime ODEs occurring at both Utqiaġvik and Oliktok Point simultaneously informs ODE spatial extents. Example ODEs from spring 2020 are shown in Fig. 2, demonstrating concurrent ozone depletion at both sites. Of all observed ODEs, 60 ± 20% (±95% confidence interval; range of 40–92% per year) occurred concurrently at the two sites located ~260 km apart. The potential for some ODEs to occur concurrently could not be determined due to missing data at either site. In such cases, the corresponding ODEs were included in the total ODE counts at each site but not in the comparison of concurrent ODEs. When one site experienced multiple ODEs over the duration of one ODE at the other site, they were counted as multiple concurrent ODEs. In Fig. 2b, for example, ozone mole ratios at Utqiaġvik recovered above 20 ppb for only 11 hours on March 4, meaning that the full period from March 1–6 constitutes one ODE according to the definitions used in this study. At Oliktok Point, however, there were two ODEs as ozone recovered above 20 ppb for 13 h. Therefore, as defined, this example was counted as two concurrent ODEs. Six instances of ODEs were observed at one site, while ozone was slightly reduced with similar temporal variability at the opposite site, but not so much as to satisfy the 15 ppb ODE threshold used in this study. For five of these six ODEs, Oliktok Point experienced an ODE, whereas ozone did not fall below the 15 ppb ODE threshold at Utqiaġvik, likely due to the lower average ozone mole ratios at Oliktok Point, as discussed in Section 3.1. If we consider these instances as concurrent "ODEs", then 70 ± 20% (range of 44–92% per year) of the ODEs at the two sites occurred concurrently. For non-concurrent ODEs, smaller spatial scales cannot necessarily be inferred since extensive ODEs may only impact one site (*e.g.*, an ODE may impact Utqiaġvik but extend much farther west rather than east toward Oliktok Point). While smaller spatial scales have been previously reported (*e.g.*, Mickle *et al.*[44]), the prevalence of concurrent ozone depletion at Utqiaġvik and Oliktok Point supports that larger ODE spatial scales of at least ~260 km are more common. These observations are

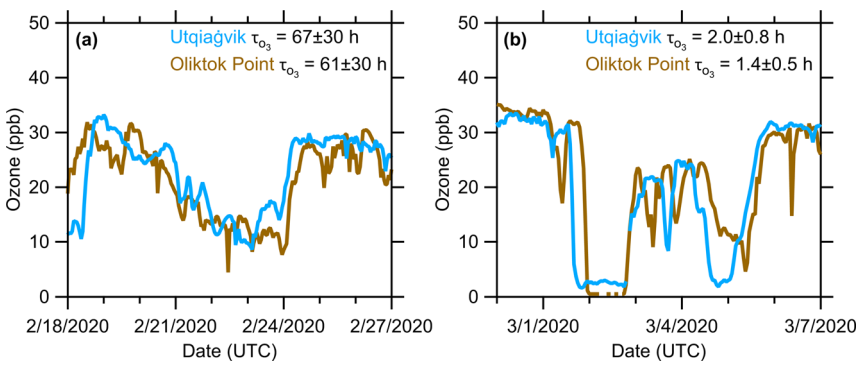

Fig. 2 Hourly ozone mole ratios (ppb) and calculated ozone depletion timescales (τ_{O_3}) at Utqiaġvik and Oliktok Point for two example coincident ODEs with (a) multi-day ozone depletion timescales, indicative of local bromine chemistry initiating the ODE,[27–30] and (b) short timescales (<24 h), indicative of air mass transport of ozone-depleted air.[5,31–33] The timescales reported in the figure correspond to the ODEs initiated on 20 February and 1 March in panels (a) and (b), respectively.

in agreement with the estimated median spatial scale of ~877 km reported by Halfacre *et al.*[31] and modelled widespread ozone depletion across the NSA reported by Cao *et al.*[117]

Wind directions at the sampling sites can provide insights into the regional air masses driving concurrent ODEs. In addition, non-concurrent ODEs at Utqiaġvik and Oliktok Point may be partially explained by sea ice lead-induced vertical mixing, where convection mixes ozone-depleted surface-level air with non-depleted air masses aloft, occurring immediately upwind of only one of the sites, as has been previously observed.[23,24] Wind directions during ODE periods were generally similar to wind directions during all of spring (Fig. S5†). Wind directions at Utqiaġvik during ODEs typically originated from the east and northeast, in the direction of the frozen Beaufort Sea (Fig. S5c†). This observation differs from that of Koo *et al.*[32] who reported ozone-depleted air masses arriving at Utqiaġvik from the Chukchi Sea to the northwest and a lack of ozone depletion in air masses from the Beaufort Sea in April 2008. Using backward air mass trajectories for ODEs observed at buoys in the Arctic Ocean north of Utqiaġvik from 2009–2011, Halfacre *et al.*[31] found ODEs primarily originated from the north (~39%), followed by the east (~33%) then the west (~22%). Different observations may simply be from differences between the time periods and locations of open sea ice leads, which terminate ODEs by downward mixing of background ozone-containing air,[23,24] or active bromine chemistry, which depends on a number of environmental factors, including surface snow pH.[118] Sea ice cover is rapidly thinning, with multiyear sea ice replaced by first year sea ice,[119–122] which has been correlated with reactive bromine chemistry.[34–37] During ODEs at Oliktok Point, the wind similarly came from the northeast, with moderate contributions (~25% of the time) from the southwest, in the direction of the tundra and some oil drilling operations (Fig. S5h†). These typical wind directions support that both Utqiaġvik and Oliktok Point typically sampled air masses from similar regions, explaining the observation of frequent concurrent ODEs.

Due to the ~260 km separation, Utqiaġvik and Oliktok Point sampled the same air masses at different times depending on the air mass arrival timing. While daily ozone mole ratios were positively correlated between the two sites ($R^2 = 0.62$; Fig. S4†), correlations on shorter timescales (<24 h) were weaker due to time offsets based on the onset of ozone depletion and subsequent recovery at each site. In Fig. 2, the average wind direction during the two example ODEs at Oliktok Point were from the southwest and southeast for the ODEs on 20 February 2020 and 1 March 2020, respectively. At Utqiaġvik, the average wind directions were from the east and southeast for the ODEs during the same time periods, respectively. HYSPLIT backward air mass trajectories (Fig. S7†) suggest that the air masses associated with these example ODEs broadly originated from the southwest over the tundra and otherwise followed similar trajectories before arriving at each site. Therefore, HYSPLIT analysis supports that both Utqiaġvik and Oliktok Point were impacted by the same air masses during these example ODEs. These westerly air masses are expected to reach Utqiaġvik first, yielding ozone depletion sooner than at Oliktok Point, in agreement with observations showing ozone depletion and recovery ~6 h sooner at Utqiaġvik compared to Oliktok Point (Fig. 2).

Ozone depletion timescales provide ODE kinetic information and inform whether ozone depletion was initiated by local bromine chemistry.[27–31] Observed

timescales of ozone depletion ranged from ~2 h to ~5 days at Utqiaġvik and <1 h to ~2.5 days at Oliktok Point (Fig. S8†). Based on typically observed BrO˙ mole ratios and rate coefficients, ozone depletion *via* local bromine chemistry is estimated to occur on timescales of a day or longer.[27–30] Therefore, to compare the prevalence of these timescales, we separate short (≤24 h) and long (24–48 h) ozone depletion timescales (τ_{O_3}), indicative of transport of ozone-depleted air and ozone depletion initiated by local bromine chemistry, respectively. Most ODEs occurred on short timescales at both sites: on average 76% (range of 62–91% during individual years) of ODEs at Utqiaġvik and 82% (72–94%) at Oliktok Point. An average of 19% (9–38% each year) and 15% (0–25%) of ODEs occurred on long (24–48 h) timescales at Utqiaġvik and Oliktok Point, respectively. Longer ODE timescales (>48 h) occurred at most once during any given year at each site and are indicative of poor mixing with ozone-rich air.[25,31] The median ODE timescales observed at Utqiaġvik and Oliktok Point were 11 h and 9 h, respectively, in agreement with the 11 h median reported by Halfacre *et al.*[31] using buoy measurements over the Arctic Ocean. The prevalence of shorter timescales supports the concurrent transport of ozone-depleted air masses to these sites, as has been previously observed at Utqiaġvik.[32] Concurrent ODEs observed at these sites with similar timescales also support the large spatial scales of ozone depletion previously predicted by Halfacre *et al.*[31] through backward air mass trajectories. Utqiaġvik and Oliktok Point shared ODEs with short ozone depletion timescales (Fig. 2b), suggesting widespread ozone depletion upwind. They also shared ODEs on longer timescales (Fig. 2a), suggesting widespread active bromine chemistry, in agreement with observations of elevated BrO˙ across broad snow-covered regions of the Arctic during spring.[32,123–125]

Once ozone is depleted, atmospheric oxidative capacity is reduced for the duration of the ODE. Both sites experienced a similar distribution of ODE durations from 2017–2021 (Fig. S9†). Durations of ODEs ranged from 12–292 h (median of 51 h) and 12–296 h (median of 55 h) at Utqiaġvik and Oliktok Point, respectively, over the study period (2017–2021). In comparison, Halfacre *et al.*[31] reported a median duration of ~70 h for buoy measurements in consolidated sea ice of the Arctic Ocean. In comparison, our study utilized coastal sites that are likely more impacted by open sea ice leads that cause recovery of ozone background levels through enhanced atmospheric mixing.[23,24] Each site experienced a similar number of ODEs with durations of less than 2 days (27 total ODEs during the study period at both sites; 4–6 and 3–7 per year at Utqiaġvik and Oliktok Point, respectively) as the number of ODEs with durations of 2–4 days (31 total ODEs during the study period, 3–12 per year, at Utqiaġvik; 31 total ODEs, 4–10 per year, at Oliktok Point). A smaller number of ODEs, 6 at Utqiaġvik and 7 at Oliktok Point, lasted longer than a week, with the longest ODE being sustained over 12 days. All ODEs with long durations occurred concurrently at both sites. In comparison, the longest ODE reported by Halfacre *et al.*[31] lasted for ~14.5 days. For some ODEs in our study, ozone was able to recover above 20 ppb briefly (<24 h) before initiating a separate ODE. In a subset of these cases, either site would experience one long ODE, while the other experienced two shorter ODEs. These long periods of depleted ozone suggest a combination of poor mixing on these timescales and large ODE spatial scales as the depleted air masses are transported over the sites.

Following long-term observations of Arctic ODEs, Tarasick and Bottenheim[126] proposed that low temperatures (<−20 °C) may be necessary to initiate ODEs. HOBr is efficiently taken up by frozen surfaces (<−20 °C) to regenerate Br_2 *via* **R4**,[127] and increasing BrO˙ mole ratios have been correlated with decreasing temperatures below −15 °C.[128] In contrast, Peterson *et al.*[42] found no clear trend between temperature and BrO˙ mole ratios during an airborne campaign near Utqiaġvik; however, ambient temperatures only reached a maximum of −20 °C. Custard *et al.*[12] reported enhanced snowpack Br_2 emissions at air temperatures up to −14 °C compared to higher temperatures, but noted that the corresponding snowpack temperatures were likely lower. For the current study, the distributions of ambient temperatures during ODEs (averaged from ODE_{start} to ODE_{stop}) at each site were similar to those distributions for all of spring (Fig. S9†). However, average hourly temperatures (±95% confidence intervals) during ODEs (−19.2 ± 0.5 °C at Utqiaġvik and −20.4 ± 0.7 °C at Oliktok Point) were statistically lower compared to the spring averages (−17.3 ± 0.2 °C and −18.3 ± 0.2 °C) at both sites. ODEs were observed at ambient temperatures ranging from −38.5 ± 0.6 °C to −2.2 ± 0.2 °C (median of −19.0 ± 0.3 °C) across both sites. However, the temperature of the airmass at the time of measurement could be different from the temperature when ozone was actively depleted by bromine chemistry upwind. When only considering ODEs on moderate timescales (24–48 h; indicative of local bromine chemistry),[27–30] temperatures were over the same range (−38.5 ± 0.6 °C to −2.2 ± 0.2 °C; median of −18.56 ± 0.01 °C), representing an insignificant difference from the distribution of all ODEs. Moreover, Halfacre *et al.*[31] reported no significant difference between ambient temperatures measured at their measurement sites (buoys in the Arctic Ocean) and the average temperature of isobaric backward air mass trajectories, most of which remained near the surface (<200 m). These observations are in agreement with many studies reporting ODEs occurring at warmer temperatures (>−20 °C) and not being restricted to only the lower temperature range.[31,32,34,129]

Reactive bromine chemistry has been associated with low wind speeds (<8 m s^{-1}) with stable boundary layer conditions in which the bromine explosion cycle is efficient,[14] as well as high wind speeds (>8 m s^{-1}) with bromine release suggested from sublimated blowing snow.[124,130,131] Swanson *et al.*[130] observed ODEs during both calm winds and blowing snow at Utqiaġvik and on buoys in the Arctic Ocean from 2009–2015, but found an average wind speed of 5.6 m s^{-1}, which falls in the calm wind regime. Additional studies have also observed elevated near-surface reactive bromine (Br_2, HOBr, BrO˙) during periods of calm winds (*e.g.*, Helmig *et al.*,[132] Peterson *et al.*,[133] Wang *et al.*[11]). For the current study, median wind speeds during all ODEs were 5.0 ± 0.2 m s^{-1} at Utqiaġvik and 5.6 ± 0.2 m s^{-1} at Oliktok Point, and most ODEs (83% at Utqiaġvik and 79% at Oliktok Point) occurred during calm winds below 8 m s^{-1} (Fig. 3). For ODEs with 24–48 h timescales, consistent with local bromine-driven ozone depletion, 75% had average wind speeds below 8 m s^{-1} (range of 1.14 ± 0.08 m s^{-1} to 10.7 ± 0.2 m s^{-1}; median of 5.3 ± 0.2 m s^{-1}). Wind speeds were not statistically different (95% confidence) between the two sites during ODEs, but ODE wind speeds were significantly slower compared to all of spring, on average, by 0.4 m s^{-1} at Utqiaġvik and 0.7 m s^{-1} at Oliktok Point. As with the temperature comparison, the wind speeds at the measurement site may not be representative of the wind speeds at the time of ozone depletion in the air mass. ODE observations presented

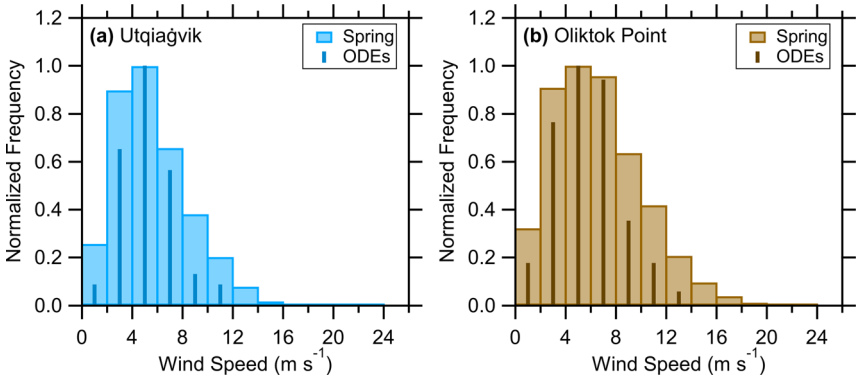

Fig. 3 Normalized histograms of hourly averaged wind speeds measured at (a) Utqiaġvik and (b) Oliktok Point for all springtime data and all springtime ODE data. Wind speeds were grouped into 2 m s^{-1} bins. ODE wind speeds were averaged across the duration of each ODE (ODE_{start} to ODE_{stop}). Since ODEs represent a smaller subset of spring, the histograms are normalized to better compare the distributions. For both sites, wind speeds were slower during ODEs (95% confidence).

here and reported elsewhere support that blowing snow is not required for ODEs, and that near-surface ozone depletion and reactive bromine chemistry during calm wind conditions are more prevalent.[31,130,132]

3.3 Influence from anthropogenic NO_x from Arctic oil field extraction emissions

The Oliktok Point field site is surrounded by drilling platforms within 2 km to the east, southeast, and south, with other sites slightly farther away in all directions including offshore platforms to the north. Unfortunately, no NO_x measurements were available at Oliktok Point during this study period. However, Oliktok Point experiences constant influence from oil field emissions, including NO_x, and few periods of "clean", non-polluted air.[71] Utqiaġvik also experiences intermittent NO_x pollution, transported from the town of Utqiaġvik, ~5 km to the southwest, as well as the NSA oil fields, ~300 km to the southeast.[62,73–75] Therefore, ozone titration by $NO^{\bullet}$ (R5) likely contributes to lower ozone mole ratios at Oliktok Point compared to Utqiaġvik.

While daily ozone mole ratios were correlated between the two sites during this study, ozone at Oliktok Point was typically a few ppb lower than at Utqiaġvik (Fig. S1 and S4†). When comparing seasons, average ozone mole ratios (±95% confidence intervals) were statistically lower at Oliktok Point by 3.8 ± 0.1 ppb in winter, 2.9 ± 0.3 ppb in spring, 3.5 ± 0.2 ppb in summer, and 6.1 ± 0.2 ppb in fall (Fig. 1a). The two sites most closely agreed in February (ozone mole ratio difference of 2.4 ± 0.5 ppb, ~9% lower ozone at Oliktok Point; Fig. 1b), likely due to the prevalence of halogen chemistry controlling ozone mole ratios as opposed to NO_x. The largest difference was observed in August (6.8 ± 0.3 ppb, ~27% lower ozone at Oliktok Point), potentially related to iodine or VOC chemistry, in addition to NO_x influence, as discussed in Section 3.1. At Utqiaġvik, Jaffe *et al.*[73] reported pollution events with NO_x up to ~14 ppb nearly 300 km downwind from the NSA oil fields. Thus, given that Oliktok Point is within the oil fields, it is expected that

local NO˙ mole ratios are sufficient to titrate ~3–7 ppb ozone (R5) and account for this observed ozone difference compared to Utqiaġvik.

Ozone titration by NO˙ (R5) and the lower average ozone mole ratios at Oliktok Point in spring also influenced ODE characteristics (Section 3.2). With lower average ozone mole ratios, ozone was slower to recover above the 20 ppb threshold used to signify an ODE end time. Therefore, a greater proportion of spring was considered ozone depleted at Oliktok Point (40%) compared to Utqiaġvik (35%). ODEs at Oliktok point also tended to have a longer duration (Fig. S9†). While both sites experienced a similar number of ODEs, a greater fraction of ODEs at Oliktok Point happened on shorter ozone depletion timescales (≤24 h; Fig. S8†). Frequent, short-term ozone variability at Oliktok Point coinciding with a lack of variability at Utqiaġvik (Fig. 4) suggests local rather than regional influences with some ODEs induced by local NO˙ titration, potentially alongside local bromine chemistry. Similar short-term ozone titration was observed at Utqiaġvik when NO_x pollution was transported from the town or the NSA oil fields to the measurement site,[62,75] but less frequently. Hourly ozone observations were most correlated between Utqiaġvik and Oliktok Point during spring, when bromine-driven ozone depletion is most active ($R^2 = 0.56$, as compared to 0.36, 0.31, 0.14 in fall, summer, and winter, respectively). Given the stronger correlation during spring with active bromine chemistry, the short-term ozone reductions at either site are less likely to have occurred due to local-scale bromine chemistry. Weaker correlations during other seasons, with reduced or no active bromine chemistry, point toward differences in other local factors, such as NO˙ titration, driving short-term ozone reductions.

Periods of depleted ozone were also observed throughout the year at both Utqiaġvik and Oliktok Point (*e.g.*, outliers in Fig. 1a). As discussed in Section 2.2, the term "ODE" is associated with springtime, bromine-driven ozone depletion, and, therefore, we do not use this term when referring to periods of depleted ozone during other seasons. During the summer months, ozone was depleted

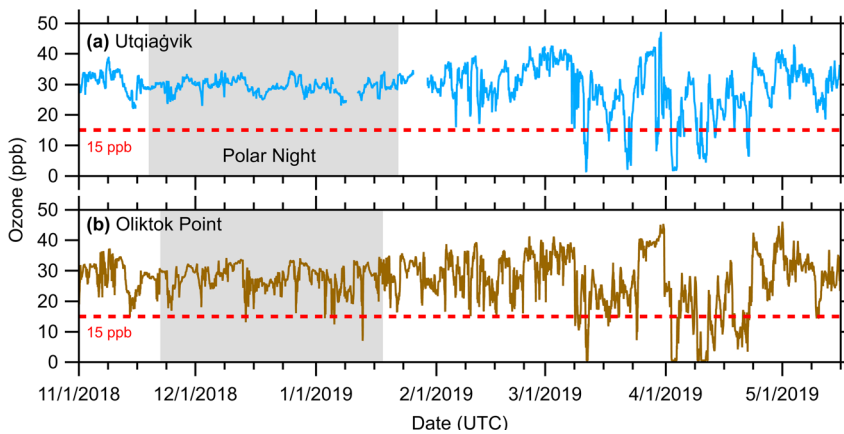

Fig. 4 Hourly ozone mole ratios during winter–spring in 2018–2019 at (a) Utqiaġvik and (b) Oliktok Point. The grey shaded regions represent the polar night at each site (nighttime > 24 h), and the red dashed lines represent the threshold used to identify ODEs.

during 18 and 29 periods according to the same definitions used to identify springtime ODEs (Section 2.2) at Utqiaġvik and Oliktok Point, respectively, with median timescales of 15 h and 11 h and median durations of 45 h and 52 h. During the fall months, there were 20 periods of depleted ozone at Utqiaġvik (median timescale of 14 h, duration of 39 h) and 50 periods at Oliktok Point (median timescale of 12 h, duration of 48 h). As with observations of springtime ODEs, periods of depleted ozone tended to happen on faster timescales and last longer at Oliktok Point. In contrast to spring, when ODEs occurred at similar frequencies at both sites, Oliktok Point experienced many more periods of depleted ozone during other seasons compared to Utqiaġvik. As such, local influences such as NO_x are the likely drivers for ozone depletion at Oliktok Point.

Depleted ozone was also observed at Oliktok Point during the polar night (22 November–18 January), in the absence of photochemistry. Using the same definitions as for the spring ODEs, four instances of ozone depletion were observed at Oliktok Point (*e.g.*, Fig. 4b), but none were identified at Utqiaġvik. The corresponding ozone depletion timescales were 1.60 ± 0.03 h, 2.9 ± 0.7 h, 3.1 ± 0.2 h, and 9 ± 3 h, with durations of 6 h, 4 h, 8 h, and 12 h, respectively. Wind primarily originated from the northeast and southwest, in the direction of active drilling platforms. Wind speeds were slower during these periods, on average ($\pm$95% confidence interval) 5 ± 1 m s^{-1} compared to 7.38 ± 0.09 m s^{-1} during all of winter at Oliktok Point. However, wind data were not available during two of the four periods. The slow wind speeds suggest poor mixing of the pollution plumes with the surrounding background ozone in air masses prior to reaching the sampling site, allowing for substantial ozone titration. Using a less stringent definition (if ozone is depleted below 15 ppb for only 1 h), there were 14 instances of depleted ozone during the polar night at Oliktok Point and still none at Utqiaġvik. These observations are notable as ozone is typically at a maximum during the winter months due to the lack of halogen photochemistry and ozone photolysis chemistry.[6,7,94] Although comparisons to springtime ODE characteristics are difficult considering the few depleted periods during polar night, the shorter timescales and durations, in combination with a lack of photochemistry, indicate ozone titration by local NO$^{\bullet}$ emissions from the NSA oil field operations.

4 Conclusions

An understanding of the factors affecting regional and local levels of the greenhouse gas ozone is especially important in the Arctic, where snow- and ice-albedo feedback amplifies radiative forcing and contributes to an increased rate of warming compared to the rest of the world.[134,135] To improve understanding of ODE characteristics, including spatial scales, we analyzed continuous ozone measurements from fall 2016 to spring 2021 at two sites, separated by $\sim$260 km, along the North Slope of Alaska: Utqiaġvik and Oliktok Point. Ozone was correlated between the two sites, demonstrating similar seasonal behavior to previous studies at Utqiaġvik. Springtime ozone depletion on the North Slope of Alaska during this study can be broadly described as follows:

(i) ODEs frequently impacted Utqiaġvik and Oliktok Point concurrently (40–92% of observed ODEs each year), indicating ODE spatial scales exceeding $\sim$260 km. While smaller ODE spatial scales occur (*e.g.*, Mickle *et al.*[44]), larger spatial scales appear to be more common, in agreement with other studies reporting

larger spatial scales[45,46] and the estimated median spatial scale of ~877 km reported by Halfacre *et al.*[31]

(ii) The majority of ODEs occurred on short timescales (<24 h) due to air mass transport of ozone-depleted air from upwind, typically from the direction of the frozen Beaufort Sea to the northeast. However, some ODEs occurred on longer timescales (24–48 h), indicating ODE initiation *via* local bromine chemistry occurring on a regional scale, consistent with previous satellite and aircraft BrO˙ measurements.[42,47,48,63]

(iii) Ozone was depleted for long durations (>48 h) and for substantial fractions of the Arctic spring (35% at Utqiaġvik and 40% at Oliktok Point).

(iv) ODEs typically occurred during low wind speeds (<8 m s^{-1}; median wind speeds of 5.0 ± 0.2 m s^{-1} and 5.6 ± 0.2 m s^{-1} at Utqiaġvik and Oliktok Point, respectively), promoting a stable boundary layer conducive to bromine explosion chemistry.

(v) ODEs occurred over a wide range of temperatures (−39 °C to −2 °C); low temperatures (<−20 °C) were not necessary to allow ozone depletion chemistry.

Ozone mole ratios were lower throughout the year at Oliktok Point, with ODEs happening more frequently, on faster ozone depletion timescales, and for longer durations compared to Utqiaġvik. Oliktok Point also experienced periods of depleted ozone during the polar night in the absence of photochemistry, while Utqiaġvik did not. These observations all point to the greater ozone titration by NO˙ (R5) emitted from the oil and gas facilities surrounding the Oliktok Point site.

While not independent from bromine chemistry,[55,62,63,75] NO_x presents a different, poorly constrained pathway for ozone depletion in the Arctic. Law *et al.*[136] reported increasing surface-level ozone in the Arctic during winter from 1993–2019, attributing this increase to decreasing NO_x emissions in Europe and North America, resulting in reduced ozone titration at mid-latitudes[137] prior to transport to the Arctic.[138] However, there are substantial NO_x emissions from existing oil and gas infrastructure in the Arctic,[67,68] and the Arctic is home to 30% and 13% of the world's undiscovered gas and oil resources, respectively.[139] Increasing development and anthropogenic emissions from resource extraction and shipping in the Arctic are expected with the warming climate and melting sea ice.[76,77] Future studies should take advantage of satellite remote sensing to quantify and assess the extent of anthropogenic NO_2 emissions from oil and gas extraction activities across the Arctic, as has been done by van der A *et al.*[67] for natural gas compressor stations in Siberia and by Ialongo *et al.*[68] for gas flaring in Siberia. VOC oxidation in the presence of NO_x also plays an important role in the production of ozone downwind of pollution sources,[114,140] so detailed measurements of VOC emissions from Arctic oil and gas extraction activities are necessary to fully comprehend the impact of these activities on a regional scale. New insights into the role of anthropogenic NO_x and VOC emissions in the rapidly changing Arctic are crucial to the development of accurate climate and chemistry-transport models,[94] as well as the overall understanding of Arctic atmosphere. This study demonstrates the role of NO_x emissions from oil and gas extraction activities on local ozone and informs the impact of current and future resource extraction across the Arctic.

Data availability

This study utilized publicly available ozone and meteorological data (accessed 20 April 2021) collected at the National Oceanic and Atmospheric Administration Global Monitoring Laboratory Barrow Atmospheric Baseline Observatory at Utqiaġvik, Alaska (**http://doi.org/10.7289/V57P8WBF**),[79] and the Department of Energy Atmospheric Radiation Measurement mobile facility at Oliktok Point, Alaska (**https://doi.org/10.5439/1346692**).[80]

Author contributions

KAP conceptualized this study and advised throughout the investigation. EMW and ARJ performed the investigation, analyzed the data, visualized the results, and wrote the original draft of the manuscript. All authors contributed to manuscript revisions.

Conflicts of interest

There are no conflicts to declare.

Acknowledgements

We thank the National Science Foundation (AGS-2147893 and OPP-2000493) for funding, as well as the University of Michigan Program in International and Comparative Studies and College of Literature, Science, and the Arts for undergraduate summer research fellowships for EMW. We thank Judy Wu for programming and data analysis assistance and Kathryn Kulju, Daun Jeong, and Hannah Kenagy for discussions. We are grateful to Peter Effertz and Irina Petropavlovskikh for providing the NOAA data and for additional insight.

References

1 Intergovernmental Panel on Climate Change, *Climate Change 2021 – the Physical Science Basis: Working Group I Contribution to the Sixth Assessment Report of the Intergovernmental Panel on Climate Change*, Cambridge University Press, Cambridge, 2023.
2 J. H. Seinfeld and S. N. Pandis, *Atmospheric Chemistry and Physics: from Air Pollution to Climate Change*, Wiley, 3rd edn, 2016.
3 A. M. Thompson, The oxidizing capacity of the earth's atmosphere: probable past and future changes, *Science*, 1992, **256**, 1157–1165.
4 D. H. Ehhalt, Photooxidation of trace gases in the troposphere Plenary Lecture, *Phys. Chem. Chem. Phys.*, 1999, **1**, 5401–5408.
5 W. R. Simpson, R. von Glasow, K. Riedel, P. Anderson, P. Ariya, J. Bottenheim, J. Burrows, L. J. Carpenter, U. Frieß, M. E. Goodsite, D. Heard, M. Hutterli, H.-W. Jacobi, L. Kaleschke, B. Neff, J. Plane, U. Platt, A. Richter, H. Roscoe, R. Sander, P. Shepson, J. Sodeau, A. Steffen, T. Wagner and E. Wolff, Halogens and their role in polar boundary-layer ozone depletion, *Atmos. Chem. Phys.*, 2007, **7**, 4375–4418.

6 D. Helmig, S. J. Oltmans, D. Carlson, J.-F. Lamarque, A. Jones, C. Labuschagne, K. Anlauf and K. Hayden, A review of surface ozone in the polar regions, *Atmos. Environ.*, 2007, **41**, 5138–5161.
7 S. J. Oltmans and W. D. Komhyr, Surface ozone distributions and variations from 1973–1984: Measurements at the NOAA Geophysical Monitoring for Climatic Change Baseline Observatories, *J. Geophys. Res.:Atmos.*, 1986, **91**, 5229–5236.
8 L. A. Barrie, J. W. Bottenheim, R. C. Schnell, P. J. Crutzen and R. A. Rasmussen, Ozone destruction and photochemical reactions at polar sunrise in the lower Arctic atmosphere, *Nature*, 1988, **334**, 138–141.
9 S. J. Oltmans, Surface ozone measurements in clean air, *J. Geophys. Res.:Oceans*, 1981, **86**, 1174–1180.
10 S. J. Oltmans, B. J. Johnson and J. M. Harris, Springtime boundary layer ozone depletion at Barrow, Alaska: Meteorological influence, year-to-year variation, and long-term change, *J. Geophys. Res.:Atmos.*, 2012, **117**, D00R18, DOI: 10.1029/2011JD016889.
11 S. Wang, S. M. McNamara, C. W. Moore, D. Obrist, A. Steffen, P. B. Shepson, R. M. Staebler, A. R. W. Raso and K. A. Pratt, Direct detection of atmospheric atomic bromine leading to mercury and ozone depletion, *Proc. Natl. Acad. Sci. U. S. A.*, 2019, **116**, 14479–14484.
12 K. D. Custard, A. R. W. Raso, P. B. Shepson, R. M. Staebler and K. A. Pratt, Production and Release of Molecular Bromine and Chlorine from the Arctic Coastal Snowpack, *ACS Earth Space Chem.*, 2017, **1**, 142–151.
13 K. L. Foster, R. A. Plastridge, J. W. Bottenheim, P. B. Shepson, B. J. Finlayson-Pitts and C. W. Spicer, The Role of Br_2 and BrCl in Surface Ozone Destruction at Polar Sunrise, *Science*, 2001, **291**, 471–474.
14 K. A. Pratt, K. D. Custard, P. B. Shepson, T. A. Douglas, D. Pöhler, S. General, J. Zielcke, W. R. Simpson, U. Platt, D. J. Tanner, L. Gregory Huey, M. Carlsen and B. H. Stirm, Photochemical production of molecular bromine in Arctic surface snowpacks, *Nat. Geosci.*, 2013, **6**, 351–356.
15 S.-M. Fan and D. J. Jacob, Surface ozone depletion in Arctic spring sustained by bromine reactions on aerosols, *Nature*, 1992, **359**, 522–524.
16 R. Vogt, P. J. Crutzen and R. Sander, A mechanism for halogen release from sea-salt aerosol in the remote marine boundary layer, *Nature*, 1996, **383**, 327–330.
17 C. R. Thompson, P. B. Shepson, J. Liao, L. G. Huey, E. C. Apel, C. A. Cantrell, F. Flocke, J. Orlando, A. Fried, S. R. Hall, R. S. Hornbrook, D. J. Knapp, R. L. Mauldin III, D. D. Montzka, B. C. Sive, K. Ullmann, P. Weibring and A. Weinheimer, Interactions of bromine, chlorine, and iodine photochemistry during ozone depletions in Barrow, Alaska, *Atmos. Chem. Phys.*, 2015, **15**, 9651–9679.
18 J. C. McConnell, G. S. Henderson, L. Barrie, J. Bottenheim, H. Niki, C. H. Langford and E. M. J. Templeton, Photochemical bromine production implicated in Arctic boundary-layer ozone depletion, *Nature*, 1992, **355**, 150–152.
19 J. Liao, L. G. Huey, D. J. Tanner, F. M. Flocke, J. J. Orlando, J. A. Neuman, J. B. Nowak, A. J. Weinheimer, S. R. Hall, J. N. Smith, A. Fried, R. M. Staebler, Y. Wang, J.-H. Koo, C. A. Cantrell, P. Weibring, J. Walega, D. J. Knapp, P. B. Shepson and C. R. Stephens, Observations of inorganic

bromine (HOBr, BrO, and Br_2) speciation at Barrow, Alaska, in spring 2009, *J. Geophys. Res.:Atmos.*, 2012, **117**, D00R16, DOI: 10.1029/2011JD016641.

20 L. Barrie and U. Platt, Arctic tropospheric chemistry: an overview, *Tellus B*, 1997, **49**, 450.

21 G. Ancellet, N. Daskalakis, J. C. Raut, D. Tarasick, J. Hair, B. Quennehen, F. Ravetta, H. Schlager, A. J. Weinheimer, A. M. Thompson, B. Johnson, J. L. Thomas and K. S. Law, Analysis of the latitudinal variability of tropospheric ozone in the Arctic using the large number of aircraft and ozonesonde observations in early summer 2008, *Atmos. Chem. Phys.*, 2016, **16**, 13341–13358.

22 X.-M. Hu, F. Zhang, G. Yu, J. D. Fuentes and L. Wu, Contribution of mixed-phase boundary layer clouds to the termination of ozone depletion events in the Arctic, *Geophys. Res. Lett.*, 2011, **38**, L21801, DOI: 10.1029/2011GL049229.

23 C. W. Moore, D. Obrist, A. Steffen, R. M. Staebler, T. A. Douglas, A. Richter and S. V. Nghiem, Convective forcing of mercury and ozone in the Arctic boundary layer induced by leads in sea ice, *Nature*, 2014, **506**, 81–84.

24 P. K. Peterson, K. A. Pratt, W. R. Simpson, S. V. Nghiem, L. X. Pérez Pérez, E. J. Boone, D. Pöhler, J. Zielcke, S. General, P. B. Shepson, U. Frieß, U. Platt and B. H. Stirm, The role of open lead interactions in atmospheric ozone variability between Arctic coastal and inland sites, *Elem. Sci. Anth.*, 2016, **4**, 000109.

25 C. Strong, J. D. Fuentes, R. E. Davis and J. W. Bottenheim, Thermodynamic attributes of Arctic boundary layer ozone depletion, *Atmos. Environ.*, 2002, **36**, 2641–2652.

26 H.-W. Jacobi, S. Morin and J. W. Bottenheim, Observation of widespread depletion of ozone in the springtime boundary layer of the central Arctic linked to mesoscale synoptic conditions, *J. Geophys. Res.:Atmos.*, 2010, **115**, D17302, DOI: 10.1029/2010JD013940.

27 M. Hausmann and U. Platt, Spectroscopic measurement of bromine oxide and ozone in the high Arctic during Polar Sunrise Experiment 1992, *J. Geophys. Res.:Atmos.*, 1994, **99**, 25399–25413.

28 M. Piot and R. von Glasow, The potential importance of frost flowers, recycling on snow, and open leads for ozone depletion events, *Atmos. Chem. Phys.*, 2008, **8**, 2437–2467.

29 M. Piot and R. von Glasow, Modelling the multiphase near-surface chemistry related to ozone depletions in polar spring, *J. Atmos. Chem.*, 2009, **64**, 77–105.

30 M. Tuckermann, R. Ackermann, C. Gölz, H. Lorenzen-Schmidt, T. Senne, J. Stutz, B. Trost, W. Unold and U. Platt, DOAS-observation of halogen radical-catalysed arctic boundary layer ozone destruction during the ARCTOC-campaigns 1995 and 1996 in Ny-Ålesund, Spitsbergen, *Tellus, Ser. B: Chem. Phys. Meteorol.*, 1997, **49**, 533–555.

31 J. W. Halfacre, T. N. Knepp, P. B. Shepson, C. R. Thompson, K. A. Pratt, B. Li, P. K. Peterson, S. J. Walsh, W. R. Simpson, P. A. Matrai, J. W. Bottenheim, S. Netcheva, D. K. Perovich and A. Richter, Temporal and spatial characteristics of ozone depletion events from measurements in the Arctic, *Atmos. Chem. Phys.*, 2014, **14**, 4875–4894.

32 J.-H. Koo, Y. Wang, T. P. Kurosu, K. Chance, A. Rozanov, A. Richter, S. J. Oltmans, A. M. Thompson, J. W. Hair, M. A. Fenn, A. J. Weinheimer,

T. B. Ryerson, S. Solberg, L. G. Huey, J. Liao, J. E. Dibb, J. A. Neuman, J. B. Nowak, R. B. Pierce, M. Natarajan and J. Al-Saadi, Characteristics of tropospheric ozone depletion events in the Arctic spring: analysis of the ARCTAS, ARCPAC, and ARCIONS measurements and satellite BrO observations, *Atmos. Chem. Phys.*, 2012, **12**, 9909–9922.

33 S. Morin, G. Hönninger, R. M. Staebler and J. W. Bottenheim, A high time resolution study of boundary layer ozone chemistry and dynamics over the Arctic Ocean near Alert, Nunavut, *Geophys. Res. Lett.*, 2005, **32**, L08809, DOI: **10.1029/2004GL022098**.

34 J. W. Bottenheim, S. Netcheva, S. Morin and S. V. Nghiem, Ozone in the boundary layer air over the Arctic Ocean: measurements during the TARA transpolar drift 2006–2008, *Atmos. Chem. Phys.*, 2009, **9**, 4545–4557.

35 J. B. Gilman, J. F. Burkhart, B. M. Lerner, E. J. Williams, W. C. Kuster, P. D. Goldan, P. C. Murphy, C. Warneke, C. Fowler, S. A. Montzka, B. R. Miller, L. Miller, S. J. Oltmans, T. B. Ryerson, O. R. Cooper, A. Stohl and J. A. de Gouw, Ozone variability and halogen oxidation within the Arctic and sub-Arctic springtime boundary layer, *Atmos. Chem. Phys.*, 2010, **10**, 10223–10236.

36 P. K. Peterson, W. R. Simpson and S. V. Nghiem, Variability of bromine monoxide at Barrow, Alaska, over four halogen activation (March–May) seasons and at two on-ice locations, *J. Geophys. Res.:Atmos.*, 2016, **121**, 1381–1396.

37 W. R. Simpson, D. Carlson, G. Hönninger, T. A. Douglas, M. Sturm, D. Perovich and U. Platt, First-year sea-ice contact predicts bromine monoxide (BrO) levels at Barrow, Alaska better than potential frost flower contact, *Atmos. Chem. Phys.*, 2007, **7**, 621–627.

38 I. Bougoudis, A.-M. Blechschmidt, A. Richter, S. Seo, J. P. Burrows, N. Theys and A. Rinke, Long-term time series of Arctic tropospheric BrO derived from UV–VIS satellite remote sensing and its relation to first-year sea ice, *Atmos. Chem. Phys.*, 2020, **20**, 11869–11892.

39 L. Kaleschke, A. Richter, J. Burrows, O. Afe, G. Heygster, J. Notholt, A. M. Rankin, H. K. Roscoe, J. Hollwedel, T. Wagner and H.-W. Jacobi, Frost flowers on sea ice as a source of sea salt and their influence on tropospheric halogen chemistry, *Geophys. Res. Lett.*, 2004, **31**, L16114, DOI: **10.1029/2004GL020655**.

40 T. Zeng, Y. Wang, K. Chance, E. V. Browell, B. A. Ridley and E. L. Atlas, Widespread persistent near-surface ozone depletion at northern high latitudes in spring, *Geophys. Res. Lett.*, 2003, **30**, 2298, DOI: **10.1029/2003GL018587**.

41 T. Zeng, Y. Wang, K. Chance, N. Blake, D. Blake and B. Ridley, Halogen-driven low-altitude O_3 and hydrocarbon losses in spring at northern high latitudes, *J. Geophys. Res.:Atmos.*, 2006, **111**, D17313, DOI: **10.1029/2005JD006706**.

42 P. K. Peterson, D. Pöhler, J. Zielcke, S. General, U. Frieß, U. Platt, W. R. Simpson, S. V. Nghiem, P. B. Shepson, B. H. Stirm and K. A. Pratt, Springtime Bromine Activation over Coastal and Inland Arctic Snowpacks, *ACS Earth Space Chem.*, 2018, **2**, 1075–1086.

43 B. Van Dam, D. Helmig, J. F. Burkhart, D. Obrist and S. J. Oltmans, Springtime boundary layer O_3 and GEM depletion at Toolik Lake, Alaska, *J. Geophys. Res.:Atmos.*, 2013, **118**, 3382–3391.

44 R. E. Mickle, J. W. Bottenheim, W. R. Leaitch and W. Evans, Boundary layer ozone depletion during AGASP-II, *Atmos. Environ. (1967-1989)*, 1989, **23**, 2443–2449.

45 W. R. Leaitch, L. A. Barrie, J. W. Bottenheim and S. M. Li, Airborne observations related to ozone depletion at polar sunrise, *J. Geophys. Res.:Atmos.*, 1994, **99**, 25499–25517.

46 B. A. Ridley, E. L. Atlas, D. D. Montzka, E. V. Browell, C. A. Cantrell, D. R. Blake, N. J. Blake, L. Cinquini, M. T. Coffey, L. K. Emmons, R. C. Cohen, R. J. DeYoung, J. E. Dibb, F. L. Eisele, F. M. Flocke, A. Fried, F. E. Grahek, W. B. Grant, J. W. Hair, J. W. Hannigan, B. J. Heikes, B. L. Lefer, R. L. Mauldin, J. L. Moody, R. E. Shetter, J. A. Snow, R. W. Talbot, J. A. Thornton, J. G. Walega, A. J. Weinheimer, B. P. Wert and A. J. Wimmers, Ozone depletion events observed in the high latitude surface layer during the TOPSE aircraft program, *J. Geophys. Res.:Atmos.*, 2003, **108**, 4109.

47 U. Platt and T. Wagner, Satellite mapping of enhanced BrO concentrations in the troposphere, *Nature*, 1998, **395**, 486–490.

48 S. Seo, A. Richter, A.-M. Blechschmidt, I. Bougoudis and J. P. Burrows, First high-resolution BrO column retrievals from TROPOMI, *Atmos. Meas. Tech.*, 2019, **12**, 2913–2932.

49 S. Sillman, The relation between ozone, NO_x and hydrocarbons in urban and polluted rural environments, *Atmos. Environ.*, 1999, **33**, 1821–1845.

50 A. Dekhtyareva, M. Hermanson, A. Nikulina, O. Hermansen, T. Svendby, K. Holmén and R. G. Graversen, Springtime nitrogen oxides and tropospheric ozone in Svalbard: results from the measurement station network, *Atmos. Chem. Phys.*, 2022, **22**, 11631–11656.

51 S. Morin, J. Savarino, M. M. Frey, N. Yan, S. Bekki, J. W. Bottenheim and J. M. F. Martins, Tracing the Origin and Fate of NO_x in the Arctic Atmosphere Using Stable Isotopes in Nitrate, *Science*, 2008, **322**, 730–732.

52 S. Morin, J. Erbland, J. Savarino, F. Domine, J. Bock, U. Friess, H.-W. Jacobi, H. Sihler and J. M. F. Martins, An isotopic view on the connection between photolytic emissions of NO_x from the Arctic snowpack and its oxidation by reactive halogens, *J. Geophys. Res.:Atmos.*, 2012, **117**, D00R08, DOI: **10.1029/2011JD016618**.

53 L. Cao, H. Sihler, U. Platt and E. Gutheil, Numerical analysis of the chemical kinetic mechanisms of ozone depletion and halogen release in the polar troposphere, *Atmos. Chem. Phys.*, 2014, **14**, 3771–3787.

54 M. J. Evans, D. J. Jacob, E. Atlas, C. A. Cantrell, F. Eisele, F. Flocke, A. Fried, R. L. Mauldin, B. A. Ridley, B. Wert, R. Talbot, D. Blake, B. Heikes, J. Snow, J. Walega, A. J. Weinheimer and J. Dibb, Coupled evolution of BrO_x-ClO_x-HO_x-NO_x chemistry during bromine-catalyzed ozone depletion events in the arctic boundary layer, *J. Geophys. Res.:Atmos.*, 2003, **108**, 8368, DOI: **10.1029/2002JD002732**.

55 S. Wang and K. A. Pratt, Molecular Halogens Above the Arctic Snowpack: Emissions, Diurnal Variations, and Recycling Mechanisms, *J. Geophys. Res.:Atmos.*, 2017, **122**, 11991–12007.

56 A. Aguzzi and M. J. Rossi, Heterogeneous Hydrolysis and Reaction of $BrONO_2$ and Br_2O on Pure Ice and Ice Doped with HBr, *J. Phys. Chem. A*, 2002, **106**, 5891–5901.

57 D. R. Hanson, Reactivity of $BrONO_2$ and HOBr on sulfuric acid solutions at low temperatures, *J. Geophys. Res.:Atmos.*, 2003, **108**, 4239, DOI: 10.1029/2002JD002519.
58 D. R. Hanson, A. R. Ravishankara and E. R. Lovejoy, Reaction of $BrONO_2$ with H_2O on submicron sulfuric acid aerosol and the implications for the lower stratosphere, *J. Geophys. Res.:Atmos.*, 1996, **101**, 9063–9069.
59 T. Thorp, S. R. Arnold, R. J. Pope, D. V. Spracklen, L. Conibear, C. Knote, M. Arshinov, B. Belan, E. Asmi, T. Laurila, A. I. Skorokhod, T. Nieminen and T. Petäjä, Late-spring and summertime tropospheric ozone and NO_2 in western Siberia and the Russian Arctic: regional model evaluation and sensitivities, *Atmos. Chem. Phys.*, 2021, **21**, 4677–4697.
60 J.-C. Raut, K. S. Law, T. Onishi, N. Daskalakis and L. Marelle, Impact of shipping emissions on air pollution and pollutant deposition over the Barents Sea, *Environ. Pollut.*, 2022, **298**, 118832.
61 C. Li, N. C. Hsu, A. M. Sayer, N. A. Krotkov, J. S. Fu, L. N. Lamsal, J. Lee and S.-C. Tsay, Satellite observation of pollutant emissions from gas flaring activities near the Arctic, *Atmos. Environ.*, 2016, **133**, 1–11.
62 K. D. Custard, C. R. Thompson, K. A. Pratt, P. B. Shepson, J. Liao, L. G. Huey, J. J. Orlando, A. J. Weinheimer, E. Apel, S. R. Hall, F. Flocke, L. Mauldin, R. S. Hornbrook, D. Pöhler, S. General, J. Zielcke, W. R. Simpson, U. Platt, A. Fried, P. Weibring, B. C. Sive, K. Ullmann, C. Cantrell, D. J. Knapp and D. D. Montzka, The NO_x dependence of bromine chemistry in the Arctic atmospheric boundary layer, *Atmos. Chem. Phys.*, 2015, **15**, 10799–10809.
63 N. Brockway, P. K. Peterson, K. Bigge, K. D. Hajny, P. B. Shepson, K. A. Pratt, J. D. Fuentes, T. Starn, R. Kaeser, B. H. Stirm and W. R. Simpson, Tropospheric bromine monoxide vertical profiles retrieved across the Alaskan Arctic in springtime, *Atmos. Chem. Phys.*, 2024, **24**, 23–40.
64 I. J. Simpson, N. J. Blake, B. Barletta, G. S. Diskin, H. E. Fuelberg, K. Gorham, L. G. Huey, S. Meinardi, F. S. Rowland, S. A. Vay, A. J. Weinheimer, M. Yang and D. R. Blake, Characterization of trace gases measured over Alberta oil sands mining operations: 76 speciated C_2–C_{10} volatile organic compounds (VOCs), CO_2, CH_4, CO, NO, NO_2, NO_y, O_3 and SO_2, *Atmos. Chem. Phys.*, 2010, **10**, 11931–11954.
65 US Energy Information Administration, *Top 100 U.S. Oil and Gas Fields*, US EIA, Washington, DC, 2015.
66 US Environmental Protection Agency, *National Emissions Inventory (NEI)*, 2017, Nitrogen Oxides, https://www.epa.gov/airemissions-inventories/2017-national-emissions-inventory-neidata, accessed 26 August 2024.
67 R. J. van der A, A. T. J. de Laat, J. Ding and H. J. Eskes, Connecting the dots: NO_x emissions along a West Siberian natural gas pipeline, *npj Clim. Atmos. Sci.*, 2020, **3**, 16.
68 I. Ialongo, N. Stepanova, J. Hakkarainen, H. Virta and D. Gritsenko, Satellite-based estimates of nitrogen oxide and methane emissions from gas flaring and oil production activities in Sakha Republic, Russia, *Atmos. Environ.:X*, 2021, **11**, 100114.
69 X. Zhang, R. van der A, J. Ding, H. Eskes, J. van Geffen, Y. Yin, J. Anema, C. Vagasky, J. L. Lapierre and X. Kuang, Spaceborne Observations of Lightning NO_2 in the Arctic, *Environ. Sci. Technol.*, 2023, **57**, 2322–2332.

70 J. M. Creamean, M. Maahn, G. de Boer, A. McComiskey, A. J. Sedlacek and Y. Feng, The influence of local oil exploration and regional wildfires on summer 2015 aerosol over the North Slope of Alaska, *Atmos. Chem. Phys.*, 2018, **18**, 555–570.

71 M. J. Gunsch, J. Liu, C. E. Moffett, R. J. Sheesley, N. Wang, Q. Zhang, T. B. Watson and K. A. Pratt, Diesel Soot and Amine-Containing Organic Sulfate Aerosols in an Arctic Oil Field, *Environ. Sci. Technol.*, 2020, **54**, 92–101.

72 J. Wu, J. Liu, M. J. Gunsch, J. A. Mirrielees, C. E. Moffett, Q. Zhang, R. J. Sheesley and K. A. Pratt, Quantifying the Diversity of an Atmospheric Aerosol Population in an Arctic Oil Field on a Single-Particle Level, *J. Geophys. Res.:Atmos.*, 2024, **129**, e2024JD041001.

73 D. A. Jaffe, R. E. Honrath, J. A. Herring, S.-M. Li and J. D. Kahl, Measurements of nitrogen oxides at Barrow, Alaska during spring: Evidence for regional and northern hemispheric sources of pollution, *J. Geophys. Res.:Atmos.*, 1991, **96**, 7395–7405.

74 D. A. Jaffe, R. E. Honrath, D. Furness, T. J. Conway, E. Dlugokencky and L. P. Steele, A determination of the CH_4, NO_x and CO_2 emissions from the Prudhoe Bay, Alaska oil development, *J. Atmos. Chem.*, 1995, **20**, 213–227.

75 S. M. McNamara, A. R. W. Raso, S. Wang, S. Thanekar, E. J. Boone, K. R. Kolesar, P. K. Peterson, W. R. Simpson, J. D. Fuentes, P. B. Shepson and K. A. Pratt, Springtime Nitrogen Oxide-Influenced Chlorine Chemistry in the Coastal Arctic, *Environ. Sci. Technol.*, 2019, **53**, 8057–8067.

76 J. J. Corbett, D. A. Lack, J. J. Winebrake, S. Harder, J. A. Silberman and M. Gold, Arctic shipping emissions inventories and future scenarios, *Atmos. Chem. Phys.*, 2010, **10**, 9689–9704.

77 G. P. Peters, T. B. Nilssen, L. Lindholt, M. S. Eide, S. Glomsrød, L. I. Eide and J. S. Fuglestvedt, Future emissions from shipping and petroleum activities in the Arctic, *Atmos. Chem. Phys.*, 2011, **11**, 5305–5320.

78 J. Schmale, S. R. Arnold, K. S. Law, T. Thorp, S. Anenberg, W. R. Simpson, J. Mao and K. A. Pratt, Local Arctic Air Pollution: A Neglected but Serious Problem, *Earth's Future*, 2018, **6**, 1385–1412.

79 A. McClure-Begley, I. Petropavlovskikh and S. Oltmans, NOAA Global Monitoring Surface Ozone Network, **https://www.ncei.noaa.gov/access/metadata/landing-page/bin/iso?id=gov.noaa.ncdc:C00894**, accessed 20 April 2021.

80 S. Springston and A. Koontz, Ozone Monitor (AOSO3), Atmospheric Radiation Measurement (ARM) User Facility, Oliktok Point, Alaska, USA, DOI: **10.5439/1346692**, accessed 20 April 2021.

81 J. Uin, A. C. Aiken, M. K. Dubey, C. Kuang, M. Pekour, C. Salwen, A. J. Sedlacek, G. Senum, S. Smith, J. Wang, T. B. Watson and S. R. Springston, Atmospheric Radiation Measurement (ARM) Aerosol Observing Systems (AOS) for Surface-Based *In Situ* Atmospheric Aerosol and Trace Gas Measurements, *J. Atmos. Ocean. Technol.*, 2019, **36**, 2429–2447.

82 J. A. Burd, P. K. Peterson, S. V. Nghiem, D. K. Perovich and W. R. Simpson, Snowmelt onset hinders bromine monoxide heterogeneous recycling in the Arctic, *J. Geophys. Res.:Atmos.*, 2017, **122**, 8297–8309.

83 D. Jeong, S. M. McNamara, A. J. Barget, A. R. W. Raso, L. M. Upchurch, S. Thanekar, P. K. Quinn, W. R. Simpson, J. D. Fuentes, P. B. Shepson and K. A. Pratt, Multiphase Reactive Bromine Chemistry during Late Spring in

the Arctic: Measurements of Gases, Particles, and Snow, *ACS Earth Space Chem.*, 2022, **6**, 2877–2887.

84 G. Bernhard, C. R. Booth, J. C. Ehramjian, R. Stone and E. G. Dutton, Ultraviolet and visible radiation at Barrow, Alaska: Climatology and influencing factors on the basis of version 2 National Science Foundation network data, *J. Geophys. Res.:Atmos.*, 2007, **112**, D09101, DOI: **10.1029/2006JD007865**.

85 G. Wendler and F. Eaton, Surface radiation budget at Barrow, Alaska, *Theor. Appl. Climatol.*, 1990, **41**, 107–115.

86 R. Draxler and G. Hess, *NOAA Tech. Memo. ERL ARL-230: Description of the HYSPLIT_4 Modelling System*, NOAA Air Resources Laboratory, Silver Spring, MD, 1997.

87 G. Rolph, A. Stein and B. Stunder, Real-time Environmental Applications and Display sYstem: READY, *Environ. Model. Softw.*, 2017, **95**, 210–228.

88 A. F. Stein, R. R. Draxler, G. D. Rolph, B. J. B. Stunder, M. D. Cohen and F. Ngan, NOAA's HYSPLIT Atmospheric Transport and Dispersion Modeling System, *Bull. Am. Meteorol. Soc.*, 2015, **96**, 2059–2077, DOI: **10.1175/BAMS-D-14-00110.1**.

89 E. Kalnay, M. Kanamitsu, R. Kistler, W. Collins, D. Deaven, L. Gandin, M. Iredell, S. Saha, G. White, J. Woollen, Y. Zhu, M. Chelliah, W. Ebisuzaki, W. Higgins, J. Janowiak, K. C. Mo, C. Ropelewski, J. Wang, A. Leetmaa, R. Reynolds, R. Jenne and D. Joseph, The NCEP/NCAR 40-Year Reanalysis Project, *Bull. Am. Meteorol. Soc.*, 1996, **77**, 437–472.

90 QGIS Development Team, QGIS, **https://www.qgis.org/**, accessed 28 August 2024.

91 J. A. Seabrook, J. A. Whiteway, L. H. Gray, R. Staebler and A. Herber, Airborne lidar measurements of surface ozone depletion over Arctic sea ice, *Atmos. Chem. Phys.*, 2013, **13**, 6023–6029.

92 J. M. Harris, R. R. Draxler and S. J. Oltmans, Trajectory model sensitivity to differences in input data and vertical transport method, *J. Geophys. Res.:Atmos.*, 2005, **110**, D14109, DOI: **10.1029/2004JD005750**.

93 J. D. Kahl, A cautionary note on the use of air trajectories in interpreting atmospheric chemistry measurements, *Atmos. Environ.*, 1993, **27**, 3037–3038.

94 C. H. Whaley, K. S. Law, J. L. Hjorth, H. Skov, S. R. Arnold, J. Langner, J. B. Pernov, G. Bergeron, I. Bourgeois, J. H. Christensen, R.-Y. Chien, M. Deushi, X. Dong, P. Effertz, G. Faluvegi, M. Flanner, J. S. Fu, M. Gauss, G. Huey, U. Im, R. Kivi, L. Marelle, T. Onishi, N. Oshima, I. Petropavlovskikh, J. Peischl, D. A. Plummer, L. Pozzoli, J.-C. Raut, T. Ryerson, R. Skeie, S. Solberg, M. A. Thomas, C. Thompson, K. Tsigaridis, S. Tsyro, S. T. Turnock, K. von Salzen and D. W. Tarasick, Arctic tropospheric ozone: assessment of current knowledge and model performance, *Atmos. Chem. Phys.*, 2023, **23**, 637–661.

95 J. W. Bottenheim, A. G. Gallant and K. A. Brice, Measurements of NO_Y species and O_3 at 82° N latitude, *Geophys. Res. Lett.*, 1986, **13**, 113–116.

96 T. Tang and J. C. McConnell, Autocatalytic release of bromine from Arctic snow pack during polar sunrise, *Geophys. Res. Lett.*, 1996, **23**, 2633–2636.

97 G. P. Ayers, S. A. Penkett, R. W. Gillett, B. Bandy, I. E. Galbally, C. P. Meyer, C. M. Elsworth, S. T. Bentley and B. W. Forgan, Evidence for photochemical

control of ozone concentrations in unpolluted marine air, *Nature*, 1992, **360**, 446–449.

98 I. Bourgeois, J. Peischl, C. R. Thompson, K. C. Aikin, T. Campos, H. Clark, R. Commane, B. Daube, G. W. Diskin, J. W. Elkins, R.-S. Gao, A. Gaudel, E. J. Hintsa, B. J. Johnson, R. Kivi, K. McKain, F. L. Moore, D. D. Parrish, R. Querel, E. Ray, R. Sánchez, C. Sweeney, D. W. Tarasick, A. M. Thompson, V. Thouret, J. C. Witte, S. C. Wofsy and T. B. Ryerson, Global-scale distribution of ozone in the remote troposphere from the ATom and HIPPO airborne field missions, *Atmos. Chem. Phys.*, 2020, **20**, 10611–10635.

99 R. G. Derwent, P. G. Simmonds, S. Seuring and C. Dimmer, Observation and interpretation of the seasonal cycles in the surface concentrations of ozone and carbon monoxide at Mace Head, Ireland from 1990 to 1994, *Atmos. Environ.*, 1998, **32**, 145–157.

100 W. E. Janach, Surface ozone: Trend details, seasonal variations, and interpretation, *J. Geophys. Res.:Atmos.*, 1989, **94**, 18289–18295.

101 S. J. Oltmans and H. Levy, Seasonal cycle of surface ozone over the western North Atlantic, *Nature*, 1992, **358**, 392–394.

102 N. Benavent, A. S. Mahajan, Q. Li, C. A. Cuevas, J. Schmale, H. Angot, T. Jokinen, L. L. J. Quéléver, A.-M. Blechschmidt, B. Zilker, A. Richter, J. A. Serna, D. Garcia-Nieto, R. P. Fernandez, H. Skov, A. Dumitrascu, P. Simões Pereira, K. Abrahamsson, S. Bucci, M. Duetsch, A. Stohl, I. Beck, T. Laurila, B. Blomquist, D. Howard, S. D. Archer, L. Bariteau, D. Helmig, J. Hueber, H.-W. Jacobi, K. Posman, L. Dada, K. R. Daellenbach and A. Saiz-Lopez, Substantial contribution of iodine to Arctic ozone destruction, *Nat. Geosci.*, 2022, **15**, 770–773.

103 A. R. W. Raso, K. D. Custard, N. W. May, D. Tanner, M. K. Newburn, L. Walker, R. J. Moore, L. G. Huey, L. Alexander, P. B. Shepson and K. A. Pratt, Active molecular iodine photochemistry in the Arctic, *Proc. Natl. Acad. Sci. U. S. A.*, 2017, **114**, 10053–10058.

104 W. T. Sturges and L. A. Barrie, Chlorine, Bromine AND Iodine in arctic aerosols, *Atmos. Environ. (1967-1989)*, 1988, **22**, 1179–1194.

105 S. T. Krukowski, in *Iodine Chemistry and Applications*, John Wiley & Sons, Ltd, 2014, pp. 221–230.

106 A. V. Kudel'skiy, Forecasting petroleum prospects on the basis of amount of iodine in subsurface waters, *Int. Geol. Rev.*, 1978, **20**, 362–366.

107 A. Ozdemir, A. Sahinoglu, M. Jahangir and C. Temizel, in *Sustainable Materials for Oil and Gas Applications*, ed. C. Temizel, M. M. Sari, C. H. Canbaz, L. A. Saputelli and O. Torsæter, Gulf Professional Publishing, 2021, vol. 1, pp. 27–92.

108 F. G. Sawyer, M. F. Ohman and F. E. Lusk, IODINE FROM OIL WELL BRINES, *Ind. Eng. Chem.*, 1949, **41**, 1547–1552.

109 S. Kemball-Cook, A. Bar-Ilan, J. Grant, L. Parker, J. Jung, W. Santamaria, J. Mathews and G. Yarwood, Ozone Impacts of Natural Gas Development in the Haynesville Shale, *Environ. Sci. Technol.*, 2010, **44**, 9357–9363.

110 R. C. Schnell, S. J. Oltmans, R. R. Neely, M. S. Endres, J. V. Molenar and A. B. White, Rapid photochemical production of ozone at high concentrations in a rural site during winter, *Nat. Geosci.*, 2009, **2**, 120–122.

111 W. L. Chameides, F. Fehsenfeld, M. O. Rodgers, C. Cardelino, J. Martinez, D. Parrish, W. Lonneman, D. R. Lawson, R. A. Rasmussen, P. Zimmerman, J. Greenberg, P. Mlddleton and T. Wang, Ozone precursor relationships in the ambient atmosphere, *J. Geophys. Res.:Atmos.*, 1992, **97**, 6037–6055.

112 R. G. Derwent, M. E. Jenkin and S. M. Saunders, Photochemical ozone creation potentials for a large number of reactive hydrocarbons under European conditions, *Atmos. Environ.*, 1996, **30**, 181–199.

113 D. J. Jacob, *Introduction to Atmospheric Chemistry*, Princeton University Press, Princeton, NJ, illustrated edition, 1999.

114 K. B. Moiseenko, A. V. Vasileva, A. I. Skorokhod, Yu. A. Shtabkin, I. B. Belikov and A. Yu. Repin, Photostationary Equilibrium in the O_3–NO_x System and Ozone Generation According to ZOTTO Tall Tower Data, *Atmos. Oceanic Opt.*, 2022, **35**, S125–S132.

115 M. Gautrois, T. Brauers, R. Koppmann, F. Rohrer, O. Stein and J. Rudolph, Seasonal variability and trends of volatile organic compounds in the lower polar troposphere, *J. Geophys. Res.:Atmos.*, 2003, **108**, 4393, DOI: **10.1029/2002JD002765**.

116 J. B. Pernov, R. Bossi, T. Lebourgeois, J. K. Nøjgaard, R. Holzinger, J. L. Hjorth and H. Skov, Atmospheric VOC measurements at a High Arctic site: characteristics and source apportionment, *Atmos. Chem. Phys.*, 2021, **21**, 2895–2916.

117 L. Cao, S. Li, Y. Gu and Y. Luo, A three-dimensional simulation and process analysis of tropospheric ozone depletion events (ODEs) during the springtime in the Arctic using CMAQ (Community Multiscale Air Quality Modeling System), *Atmos. Chem. Phys.*, 2023, **23**, 3363–3382.

118 K. A. Pratt, Tropospheric Halogen Photochemistry in the Rapidly Changing Arctic, *Trends Chem.*, 2019, **1**, 545–548.

119 R. Kwok, Near zero replenishment of the Arctic multiyear sea ice cover at the end of 2005 summer, *Geophys. Res. Lett.*, 2007, **34**, L05501, DOI: **10.1029/2006GL028737**.

120 J. Maslanik, J. Stroeve, C. Fowler and W. Emery, Distribution and trends in Arctic sea ice age through spring 2011, *Geophys. Res. Lett.*, 2011, **38**, L13502, DOI: **10.1029/2011GL047735**.

121 S. V. Nghiem, Y. Chao, G. Neumann, P. Li, D. K. Perovich, T. Street and P. Clemente-Colón, Depletion of perennial sea ice in the East Arctic Ocean, *Geophys. Res. Lett.*, 2006, **33**, L17501, DOI: **10.1029/2006GL027198**.

122 S. V. Nghiem, I. G. Rigor, D. K. Perovich, P. Clemente-Colón, J. W. Weatherly and G. Neumann, Rapid reduction of Arctic perennial sea ice, *Geophys. Res. Lett.*, 2007, **34**, L19504, DOI: **10.1029/2007GL031138**.

123 Y. Chen, S. Liu, L. Zhu, S. Seo, A. Richter, X. Li, A. Ding, W. Sun, L. Shu, X. Wang, P. Valks, F. Hendrick, T. K. Koenig, R. Volkamer, B. Bai, D. Wang, D. Pu, S. Sun, J. Li, X. Zuo, W. Fu, Y. Li, P. Zhang, X. Yang and T.-M. Fu, Global Observations of Tropospheric Bromine Monoxide (BrO) Columns From TROPOMI, *J. Geophys. Res.:Atmos.*, 2023, **128**, e2023JD039091.

124 A. E. Jones, P. S. Anderson, M. Begoin, N. Brough, M. A. Hutterli, G. J. Marshall, A. Richter, H. K. Roscoe and E. W. Wolff, BrO, blizzards, and drivers of polar tropospheric ozone depletion events, *Atmos. Chem. Phys.*, 2009, **9**, 4639–4652.

125 T. Wagner, C. Leue, M. Wenig, K. Pfeilsticker and U. Platt, Spatial and temporal distribution of enhanced boundary layer BrO concentrations measured by the GOME instrument aboard ERS-2, *J. Geophys. Res.:Atmos.*, 2001, **106**, 24225–24235.

126 D. W. Tarasick and J. W. Bottenheim, Surface ozone depletion episodes in the Arctic and Antarctic from historical ozonesonde records, *Atmos. Chem. Phys.*, 2002, **2**, 197–205.

127 J. W. Adams, N. S. Holmes and J. N. Crowley, Uptake and reaction of HOBr on frozen and dry NaCl/NaBr surfaces between 253 and 233 K, *Atmos. Chem. Phys.*, 2002, **2**, 79–91.

128 D. Pöhler, L. Vogel, U. Frieß and U. Platt, Observation of halogen species in the Amundsen Gulf, Arctic, by active long-path differential optical absorption spectroscopy, *Proc. Natl. Acad. Sci. U. S. A.*, 2010, **107**, 6582–6587.

129 J. A. Neuman, J. B. Nowak, L. G. Huey, J. B. Burkholder, J. E. Dibb, J. S. Holloway, J. Liao, J. Peischl, J. M. Roberts, T. B. Ryerson, E. Scheuer, H. Stark, R. E. Stickel, D. J. Tanner and A. Weinheimer, Bromine measurements in ozone depleted air over the Arctic Ocean, *Atmos. Chem. Phys.*, 2010, **10**, 6503–6514.

130 W. F. Swanson, K. A. Graham, J. W. Halfacre, C. D. Holmes, P. B. Shepson and W. R. Simpson, Arctic Reactive Bromine Events Occur in Two Distinct Sets of Environmental Conditions: A Statistical Analysis of 6 Years of Observations, *J. Geophys. Res.:Atmos.*, 2020, **125**, e2019JD032139.

131 B. Zilker, A. Richter, A.-M. Blechschmidt, P. von der Gathen, I. Bougoudis, S. Seo, T. Bösch and J. P. Burrows, Investigation of meteorological conditions and BrO during ozone depletion events in Ny-Ålesund between 2010 and 2021, *Atmos. Chem. Phys.*, 2023, **23**, 9787–9814.

132 D. Helmig, P. Boylan, B. Johnson, S. Oltmans, C. Fairall, R. Staebler, A. Weinheimer, J. Orlando, D. J. Knapp, D. D. Montzka, F. Flocke, U. Frieß, H. Sihler and P. B. Shepson, Ozone dynamics and snow-atmosphere exchanges during ozone depletion events at Barrow, Alaska, *J. Geophys. Res.:Atmos.*, 2012, **117**, D20303, DOI: **10.1029/2012JD017531**.

133 P. K. Peterson, W. R. Simpson, K. A. Pratt, P. B. Shepson, U. Frieß, J. Zielcke, U. Platt, S. J. Walsh and S. V. Nghiem, Dependence of the vertical distribution of bromine monoxide in the lower troposphere on meteorological factors such as wind speed and stability, *Atmos. Chem. Phys.*, 2015, **15**, 2119–2137.

134 E. Post, R. B. Alley, T. R. Christensen, M. Macias-Fauria, B. C. Forbes, M. N. Gooseff, A. Iler, J. T. Kerby, K. L. Laidre, M. E. Mann, J. Olofsson, J. C. Stroeve, F. Ulmer, R. A. Virginia and M. Wang, The polar regions in a 2°C warmer world, *Sci. Adv.*, 2019, **5**, eaaw9883.

135 M. Rantanen, A. Y. Karpechko, A. Lipponen, K. Nordling, O. Hyvärinen, K. Ruosteenoja, T. Vihma and A. Laaksonen, The Arctic has warmed nearly four times faster than the globe since 1979, *Commun. Earth Environ.*, 2022, **3**, 168.

136 K. S. Law, J. L. Hjorth, J. B. Pernov, C. H. Whaley, H. Skov, M. Collaud Coen, J. Langner, S. R. Arnold, D. Tarasick, J. Christensen, M. Deushi, P. Effertz, G. Faluvegi, M. Gauss, U. Im, N. Oshima, I. Petropavlovskikh, D. Plummer, K. Tsigaridis, S. Tsyro, S. Solberg and S. T. Turnock, Arctic Tropospheric Ozone Trends, *Geophys. Res. Lett.*, 2023, **50**, e2023GL103096.

137 H. Bowman, S. Turnock, S. E. Bauer, K. Tsigaridis, M. Deushi, N. Oshima, F. M. O'Connor, L. Horowitz, T. Wu, J. Zhang, D. Kubistin and D. D. Parrish, Changes in anthropogenic precursor emissions drive shifts in the ozone seasonal cycle throughout the northern midlatitude troposphere, *Atmos. Chem. Phys.*, 2022, **22**, 3507–3524.

138 D. Hirdman, H. Sodemann, S. Eckhardt, J. F. Burkhart, A. Jefferson, T. Mefford, P. K. Quinn, S. Sharma, J. Ström and A. Stohl, Source identification of short-lived air pollutants in the Arctic using statistical analysis of measurement data and particle dispersion model output, *Atmos. Chem. Phys.*, 2010, **10**, 669–693.

139 D. L. Gautier, K. J. Bird, R. R. Charpentier, A. Grantz, D. W. Houseknecht, T. R. Klett, T. E. Moore, J. K. Pitman, C. J. Schenk, J. H. Schuenemeyer, K. Sørensen, M. E. Tennyson, Z. C. Valin and C. J. Wandrey, Assessment of Undiscovered Oil and Gas in the Arctic, *Science*, 2009, **324**, 1175–1179.

140 K. B. Moiseenko, A. V. Vasileva, A. I. Skorokhod, I. B. Belikov, A. Yu. Repin and Yu. A. Shtabkin, Regional Impact of Ozone Precursor Emissions on NO_X and O_3 Levels at ZOTTO Tall Tower in Central Siberia, *Earth Space Sci.*, 2021, **8**, e2021EA001762.